




# A Compact Dual-Polarized (CP, LP) With Dual-Feed Microstrip Patch Array for Target Detection

Ki-Baek Kim , Bang Chul Jung , Senior Member, IEEE, and Jong-Myung Woo , Member, IEEE

**Abstract**—A planar antenna is designed to replace complex structures of many rat-races and 90° hybrids used in conventional target detection antennas for receiving radar signals. The proposed antenna has 2 × 2 microstrip patch antenna arrays with dual feeding to radiate symmetric polarizations in the 9.375 GHz (X-band). The sum ( $\Sigma$ ) pattern with circular polarization is implemented through a sequence feeding at port 1. The simultaneous feeding of port 2 radiates a difference ( $\Delta$ ) pattern in all linear polarizations. Thus, the proposed antenna is compact, planar, and has a simple comparator circuit. Measurement results verify the designed prototype, showing that the antenna has a null depth of over 34.5 dB in all polarizations, a peak sum gain 4.51 dB at 9.375 GHz, and a 3 dB axial-ratio bandwidth of 160 MHz.

**Index Terms**—Dual-feed microstrip patch array, sequential feeding antenna, target detection antenna.

## I. INTRODUCTION

**T**ARGET detection antennas are used for direction finding and communication signal tracking of radar and satellite systems by using sum ( $\Sigma$ ) and difference ( $\Delta$ ) patterns [1]. In the conventional DF, target detection antennas use a cassegrain parabolic and a lens antenna. These antennas and monopulse comparators are very complex, heavy, and require high production costs. In contrast, a lightweight and low-cost microstrip structure has been developed for the monopulse antennas [2]. Various target detection antennas and comparators using the microstrip structure have been developed for the DF [2]–[13].

In [2]–[4], the structure with three quadrature hybrids (90° hybrid) and a phase delay line was proposed. In [5]–[7], the structure with antenna array and three or four rat-races (180° hybrid) was proposed. In [8], the monopulse comparator with four 180° hybrids was proposed. In [9]–[13], the structure with substrate integrated waveguide was proposed. However, the structures proposed in [2]–[13] have complex circuits such as rat-race and require spaces for monopulse comparator circuits.

Manuscript received November 12, 2019; accepted December 14, 2019. Date of publication December 20, 2019; date of current version April 17, 2020. (Corresponding author: Jong-Myung Woo.)

K.-B. Kim is with the Affiliated Institute of Electronics and Telecommunications Research Institute, Daejeon 34188, South Korea (e-mail: kbkim11@nsr.re.kr).

B. C. Jung is with the Department of Electronics Engineering, Chungnam National University, Daejeon 34134, South Korea (e-mail: bcjung@cnu.ac.kr).

J.-M. Woo is with the Department of Radio and Information Communications Engineering, Chungnam National University, Daejeon 34134, South Korea (e-mail: jmwoo@cnu.ac.kr).

Digital Object Identifier 10.1109/LAWP.2019.2961159

As a result, those structures induced large size and high cost for implementation.

On the other hand, a less complex antenna with two ports was proposed in [14] and [15], but the radiation patterns had limited polarizations and low isolation greater than  $-30$  dB between the two ports in passband.

Due to ambiguity in the detection of incoming waves, having a capable antenna to receive orthogonal circular polarized signals is necessary [16]. A broadband monopulse antenna using the conical four-arm spiral was proposed in [16] and [17]; these antennas have CP, but require a switch to radiate the sum ( $\Sigma$ ) or difference ( $\Delta$ ) pattern. Thus, the antennas in [16] and [17] are large and cannot radiate both the patterns simultaneously.

In this letter, we propose a compact type of antenna with two ports for precise target detection using dual-feed microstrip array, thereby replacing the complex comparator circuits. The designed antenna is printed on a substrate for low-profile and easy fabrication. The first port synthesizes a sum ( $\Sigma$ ) pattern with circular polarization (CP) by the sequence feeding of four microstrip patch antennas. The other port has new symmetrical feeding positions of antennas to make a difference ( $\Delta$ ) pattern for all polarizations [linear polarization (LP)], respectively. The simulated and measured results for the designed antenna are presented.

## II. ANTENNA DESIGN

### A. Radiating Structure Design

Fig. 1 shows the 2 × 2 dual-feed microstrip patch antenna array. Teflon ( $\epsilon_r = 2.5$ ) is used as the substrate, and its size is 80 (4 $\lambda$ ) mm × 80 (4 $\lambda$ ) mm (where  $\lambda$  = free-space wavelength of 9.375 GHz). The substrate has two printed sides of microstrip patch antennas (thickness = 1.6 mm) and feeding line (thickness = 0.8 mm). The 2 × 2 microstrip patch antenna array is designed in a square structure with a length of 8.7 mm to match 9.375 GHz (X-band).

Fig. 1(b) shows a cross section (A to A<sup>†</sup>) on Fig. 1(a). The antenna patch is connected to the feedline through a 0.4 mm diameter via. A hole of 0.6 mm diameter is made on the center of the ground plane to separate the vias from the ground electrically. To the right, the ground plane is extended using a 0.5 mm diameter via to connect the subminiature version A (SMA) connector of the port on the backside.

Each antenna has two feed points to form sum ( $\Sigma$ ) and difference ( $\Delta$ ) patterns. When sequentially feeding with the

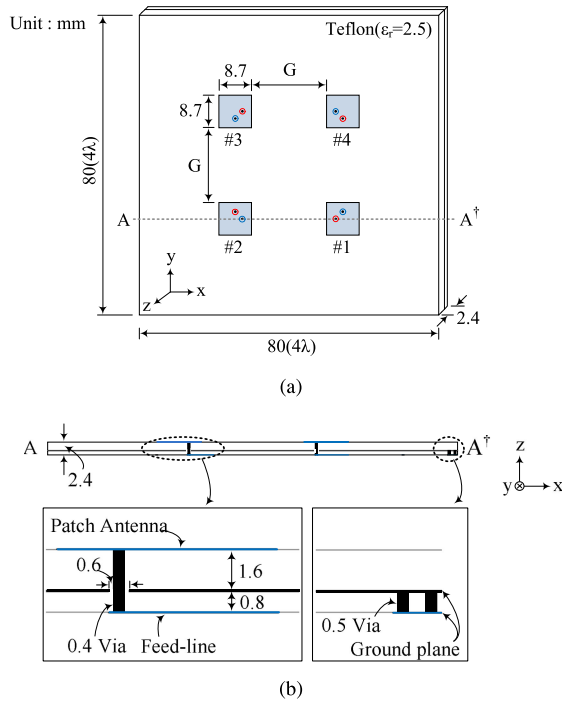


Fig. 1. Structure of the antenna. (a)  $2 \times 2$  dual-feed microstrip patch antenna array. (b) Cutting plane of A-A'.

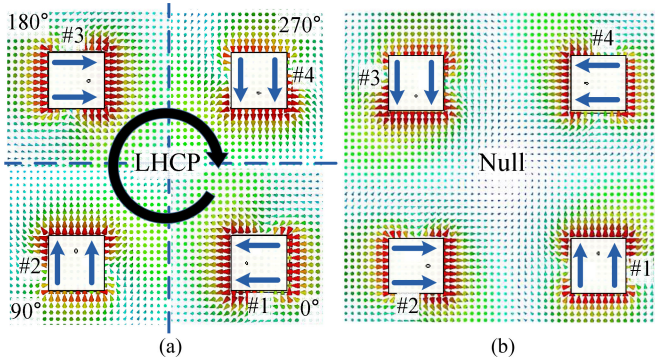


Fig. 2.  $E$ -field distribution of the antenna elements at 9.375 GHz. (a) Sequential feeding of port 1. (b) Simultaneously feeding of port 2 (in-phase).

$90^\circ$  phase difference at the feeding point marked in red from antennas 1 to 4, the electric field distribution is formed as shown in Fig. 2(a), and the sum ( $\Sigma$ ) pattern with CP is radiated.

When feeding simultaneously to the feed points marked in blue of antennas 1 to 4, the polarizations facing each other are canceled as shown in Fig. 2(b), and the difference ( $\Delta$ ) pattern with a null-point in the center of the antenna array is indicated.

Thus, CP generated from the sum ( $\Sigma$ ) pattern and LP radiated from the difference ( $\Delta$ ) pattern of the proposed antenna.

The radiation patterns of the sum ( $\Sigma$ ) and difference ( $\Delta$ ) with different gap (10–30 mm) are simulated and shown in Fig. 3. At low  $G$ , the difference ( $\Delta$ ) patterns are distorted in Fig. 3(b). Side-lobe levels (SLLs), maximum gain and half-power beamwidths (HPBW) of sum ( $\Sigma$ ) patterns are shown in Fig. 4. Higher  $G$

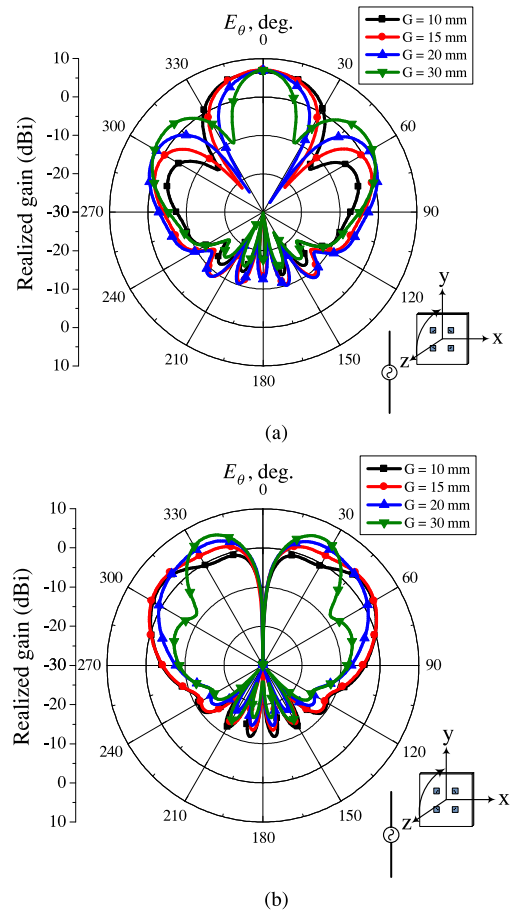


Fig. 3. Radiation patterns with gap ( $G$ ) at 9.375 GHz. (a) Sum ( $\Sigma$ ) pattern in  $yz$  plane. (b) Difference ( $\Delta$ ) pattern in  $yz$  plane.

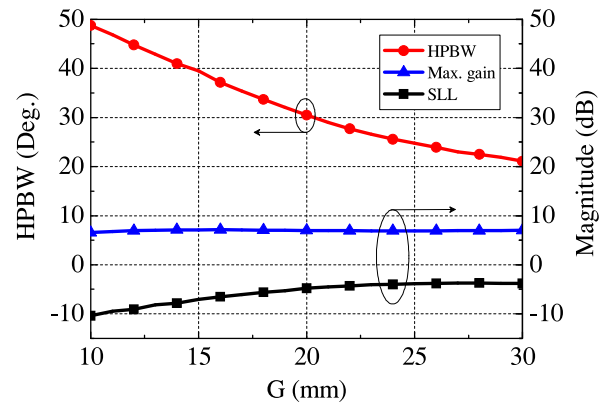


Fig. 4. HPBW, gain, and SLL of the sum ( $\Sigma$ ) pattern.

leads to increase gain and directivity, the SLLs increase, and the HPBW of sum ( $\Sigma$ ) patterns decrease. Therefore, the gap ( $G$ ) between the patch antennas is 20 mm, considering the HPBW, SLLs, and sum ( $\Sigma$ ) and difference ( $\Delta$ ) patterns.

### B. Feeding Network Design

Fig. 5(a) shows the feeding lines on the back. The two input ports are  $50 \Omega$  lines, and the impedance of the line to the antenna

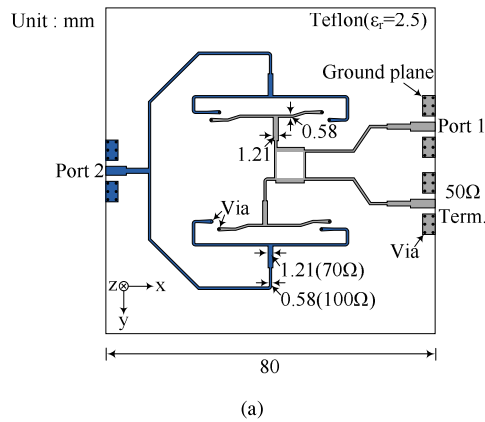


Fig. 5. Feeding network design. (a) Bottom view. (b) Feeding line of port 1.

through the T-junction power divider and  $90^\circ$  hybrid is  $100\ \Omega$  ( $0.58\ \text{mm}$ ). Port 1 is used by  $90^\circ$  hybrid and  $90^\circ$  phase delay line in the center of the antenna to provide  $180^\circ$  phase difference between the upper and bottom lines. An isolation port of  $90^\circ$  hybrid connected a  $50\ \Omega$  dummy load.

As shown in Fig. 5(b), the phase difference between points A and B over the  $90^\circ$  hybrid and phase delay ( $90^\circ$ ) line is  $180^\circ$ , respectively, with the phase difference of position C-D and E-F. Thus, the four microstrip patch antennas are designed to have sequential feeding (C-point  $0^\circ$ , D-point  $90^\circ$ , E-point  $180^\circ$ , F-point  $270^\circ$ ).

Port 2 simultaneously feeds to the antenna through T-junction power divider. Feed lines are placed in a symmetrical structure to deliver the same phase to all the four antennas. The symmetrical feeding positions of the microstrip patch antenna provide different polarizations from a single antenna.

Thus, the designed antenna can detect the direction of the movement of the target using the difference between the sum ( $\Sigma$ ) and difference ( $\Delta$ ) patterns during detection signal processing.

The results of Fig. 2 and typically target detection antennas have the sum ( $\Sigma$ ) pattern peak level of 3 dB above the difference ( $\Delta$ ) pattern peak level. In Fig. 5(b), the  $50\ \Omega$  termination load connected to the  $90^\circ$  hybrid reduces the gain of sum ( $\Sigma$ ) pattern by 3 dB. Therefore, the sum ( $\Sigma$ ) pattern level and the difference ( $\Delta$ ) pattern level of designed antenna are equal. A sequential comparison of the difference in level between the sum ( $\Sigma$ ) and the difference ( $\Delta$ ) patterns can make directional detection more effective. The fabricated antenna is shown in Fig. 6. Each port

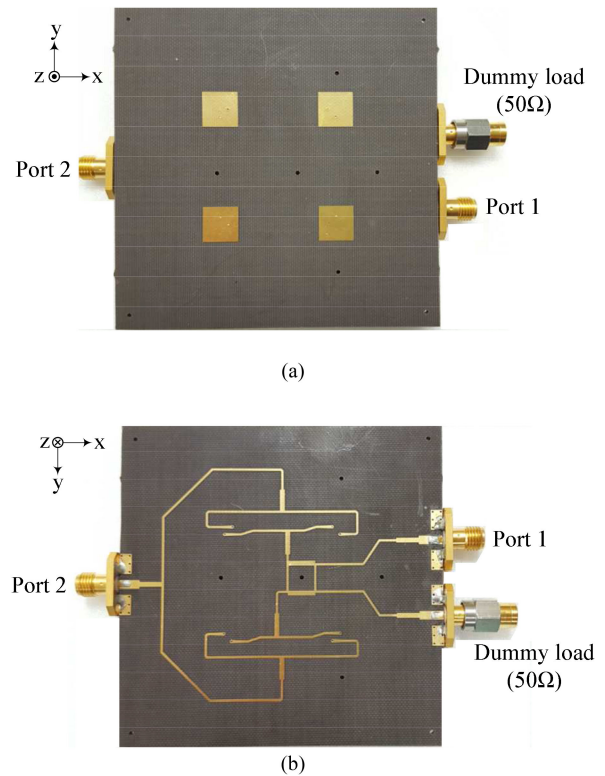


Fig. 6. Fabricated antenna. (a) Top view. (b) Bottom view.

has a  $50\ \Omega$  SMA connector and an additional  $50\ \Omega$  dummy load for an isolation port of  $90^\circ$  hybrid.

### III. SIMULATED AND MEASURED RESULTS

Fig. 7 shows a comparison of the simulated and measured radiated patterns at  $9.375\ \text{GHz}$ . A simulation is performed using CST Microwave Studio 2019 [18]. Radiation patterns were measured in an anechoic chamber under far-field conditions. Good agreement is observed between the simulation and measurement. In Fig. 7(a) and (b), the radiation pattern of sum ( $\Sigma$ ) in  $xz$  plane is shown. Fig. 7(c) and (d) shows plotting of the radiation patterns in  $yz$  plane.

The peak gain for the sum ( $\Sigma$ ) pattern was measured  $3.73\text{--}3.91\ \text{dBi}$ , and difference ( $\Delta$ ) pattern was measured  $4.30\text{--}4.51\ \text{dBi}$ . The difference ( $\Delta$ ) pattern is formed uniformly for all polarization. The proposed antenna has the same peak level of sum ( $\Sigma$ ) and difference ( $\Delta$ ) pattern.

The measured null depth is less than  $-34.5\ \text{dB}$  and the SLL are below  $-10\ \text{dB}$ . HPBW are  $22.5^\circ\text{--}40^\circ$  of sum ( $\Sigma$ ) pattern in both azimuth and elevation planes.

Fig. 8(a) shows the results of the measured  $S$ -parameters ( $S_{11}$ ,  $S_{22}$ , and  $S_{21}$ ) of ports 1 and 2. The  $-10\ \text{dB}$  bandwidth is  $185\ \text{MHz}$  ( $9.29\text{--}9.475\ \text{GHz}$ ), and isolation of two ports is  $-41.1\ \text{dB}$  at  $9.375\ \text{GHz}$ . Fig. 8(b) shows the axial ratio (AR) of the sum ( $\Sigma$ ) pattern with the simulation results. The measured 3 dB bandwidth of the AR is  $160\ \text{MHz}$  ( $9.29\text{--}9.45\ \text{GHz}$ ).

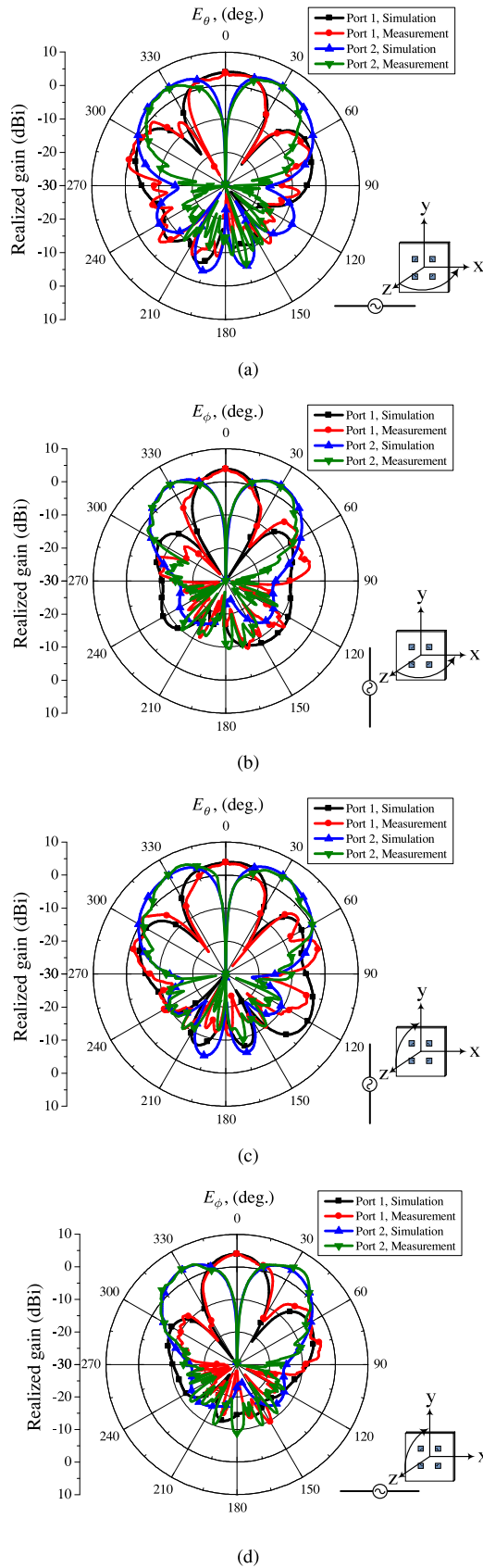
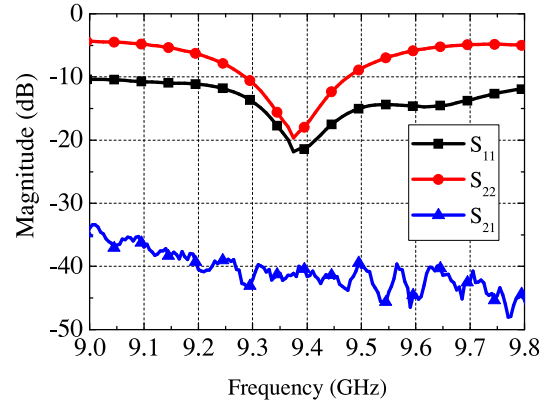
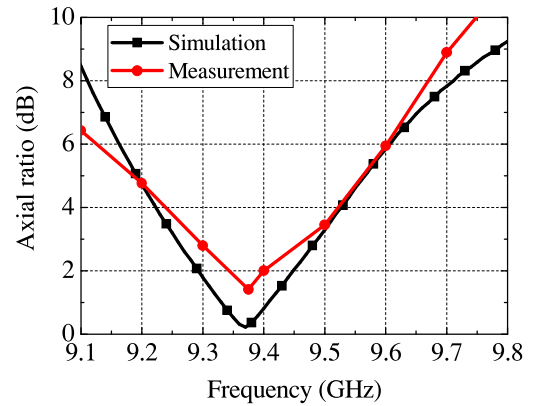


Fig. 7. Radiation patterns of proposed antenna. (a)  $E_{\theta}$  in  $xz$  plane. (b)  $E_{\phi}$  in  $xz$  plane. (c)  $E_{\theta}$  in  $yz$  plane. (d)  $E_{\phi}$  in  $yz$  plane.



(a)



(b)

Fig. 8. S-parameters and axial ratio of port 1. (a) Measured S-parameters. (b) Axial ratio.

The location of the target can be tracked by using differential value of the sum ( $\Sigma$ )/difference ( $\Delta$ ) ratio in the horizontal and vertical direction of the antenna. In addition, increasing the height of the substrate and lowering permittivity of the microstrip patch antenna can extend bandwidth for vehicle radar systems.

#### IV. CONCLUSION

A compact and planar target detection antenna for receiving radar signals is proposed in this letter, which consists of  $2 \times 2$  microstrip patch antenna array and a symmetric feeding line. The designed antenna has only two ports without rat-races and a simple comparator circuit compared with reference antennas. It has CP with the sequence feeding in 9.375 GHz ( $X$ -band) and difference ( $\Delta$ ) pattern with new simultaneous feeding in all polarizations. The measured results show that the designed antenna has achieved a good null depth of over 34.5 dB in all directions, a peak sum gain 4.51 dB at 9.375 GHz, and a 3 dB AR bandwidth of 160 MHz. Since both patterns ( $\Sigma$ ,  $\Delta$ ) are formed at the same time and equal radiation level in all polarizations, the designed antenna is suitable for receiving radar signals and target detection applications.

## REFERENCES

- [1] S. M. Sherman, *Monopulse Principles and Techniques*. Dedham, MA, USA: Artech House, 1984.
- [2] H. Wang, D.-G. Fang, and X. G. Chen, "A compact single layer monopulse microstrip antenna array," *IEEE Trans. Antennas Propag.*, vol. 54, no. 2, pp. 503–509, Feb. 2006.
- [3] J. Aliasgari and Z. Atlasbaf, "A novel compact monopulse parallel-plate slot array antenna," *IEEE Antenna Wireless Propag. Lett.*, vol. 15, pp. 762–765, 2016.
- [4] N. Yang, C. Caloz, and K. Wu, "Monopulse comparator with frequency-independent delta-channel nulls for high-resolution tracking radar," *Electron. Lett.*, vol. 47, no. 5, pp. 339–340, Mar. 2011.
- [5] H. Gharibi and F. H. Kashani, "Design of a wideband monopulse antenna using four conical helix antennas," *Prog. Electromagn. Res. Lett.*, vol. 29, pp. 25–33, Jan. 2012.
- [6] Y. L. Tsai and R. B. Hwang, "Time-division multiplexing monopulse antenna system for DVB-SH Application," *IEEE Trans. Antennas Propag.*, vol. 63, no. 2, pp. 765–769, Feb. 2015.
- [7] H. Kumar and G. Kumar, "Broadband monopulse microstrip antenna array for X-band monopulse tracking," *Microw. Antennas Propag.*, vol. 12, no. 13, pp. 2109–2114, Aug. 2018.
- [8] K. S. Ang, Y. C. Leong, and C. H. Lee, "A wide-band monopulse comparator with complete nulling in all delta channels throughout sum channel bandwidth," *IEEE Trans. Microw. Theory Techn.*, vol. 51, pp. 371–373, Feb. 2003.
- [9] H. Gharibi and F. Hodjatkashani, "Design of a compact high-efficiency circularly polarized monopulse cavity-backed substrate integrated waveguide antenna," *IEEE Trans. Antennas Propag.*, vol. 63, no. 9, pp. 4250–4256, Sep. 2015.
- [10] H. Chu, J.-X. Chen, S. Luo, and Y.-X. Guo, "A Millimeter-wave filtering monopulse antenna array based on substrate integrated waveguide technology," *IEEE Trans. Antennas Propag.*, vol. 64, no. 1, pp. 316–321, Jan. 2016.
- [11] H. Gharibi and F. H. Kashani, "Design of compact circularly polarized dual-mode monopulse cavity-backed substrate integrated waveguide antenna," *IEEE Antennas Wireless Propag. Lett.*, vol. 14, pp. 519–522, 2015.
- [12] F. Cao *et al.*, "A compact single-layer substrate-integrated waveguide (SIW) monopulse slot antenna array," *IEEE Antennas Wireless Propag. Lett.*, vol. 16, pp. 2755–2758, 2017.
- [13] Z.-C. Hao, H.-H. Wang, and W. Hong, "A novel planar reconfigurable monopulse antenna for indoor smart wireless access point's application," *IEEE Trans. Antennas Propag.*, vol. 64, no. 4, pp. 1250–1261, Apr. 2016.
- [14] F. Yu, Y. Xie, and L. Zhang, "Single patch antenna with monopulse patterns," *IEEE Microw. Wireless Compon. Lett.*, vol. 26, no. 10, pp. 762–764, Oct. 2016.
- [15] T. P. Phyeo, E. Nishiyama, and I. Toyoda, "A 5.8-GHz dual-axis monopulse microstrip array antenna using dual-feed network," in *Proc. Asia-Pac. Microw. Conf. Symp.*, Kyoto, Japan, pp. 1549–1551, Nov. 2018.
- [16] E. Mehboodi, M. Movahhedi, and A. Heidari, "Wideband dual-polarised SAW spiral antenna for monopulse system," *Microw., Antennas Propag.*, vol. 12, no. 4, pp. 607–611, Mar. 2018.
- [17] T. P. Cencich, J. C. McDonnell, and T. W. Samson, "Radiation modes of an outside fed 4-arm conical spiral," in *Proc. Int. Appl. Comput. Electromagn. Soc. Symp.*, pp. 1–2, Mar. 2018.
- [18] Microwave Studio, CST, 2019. [Online]. Available: <http://www.3ds.com>